Three-Dimensional Free-Positioning Wireless Power Transfer via Multiple-Current Amplitude Modulation

Jiahua Lyu, Wei Liu, *Senior Member, IEEE*, Shuangxia Niu, *Senior Member, IEEE*, Tianyi Liu, Songyan Niu, and K. T. Chau, *Fellow, IEEE*

***Abstract*—Free-positioning is one of the challenges for different wireless power transfer applications, from consumer electronics to industrial electronics. Misalignment leads to weak magnetic coupling and reduces the output capacity. However, much research focuses on the misalignment of the two-dimensional plane; once the transmission distance changes, the anti-misalignment capability will be weakened, and the coupler structure needs to be redesigned. This paper introduces a novel multi-current modulation method implemented on a three-layer concentric transmitter, which ensures uniform magnetic fields at varying transmission distances by modulating the current to achieve three-dimensional free-positioning. A surrogate-assisted multi-fidelity genetic algorithm is proposed to obtain the suitable coupler structure and the current amplitude for various transmission distances. A fitness function with a scoring mechanism is adopted to evaluate the uniformity of the magnetic field, which is convenient for the optimization process. Experiments are implemented to verify the anti-misalignment performance at various transmission distances. The results show that the proposed scheme exhibits 25%, 25%, and 15.6% anti-misalignment capabilities in the x, y, and z directions, respectively, and can limit the voltage fluctuation within 5.51%.**

***Index Terms*—Multiple transmitters, optimal design, planar coil, uniform magnetic field distribution, wireless power transfer.**

I. Introduction

WIRELESS power transfer (WPT) has been widely applied in consumer electronics such as portable devices, household devices, drones [1–3], and industrial electronics such as robotics and electrical vehicles [4, 5]. This technology provides convenience to users by transferring energy through magnetic coupling. There are still many challenges that need to be solved in the development and application of WPT. A significant challenge in this field is the misalignment problem, which substantially reduces output performance and necessitates precise alignment between the receiver's position and the transmitter's center. The problem reduces the convenience of the technology and hinders the development of WPT functions such as the multi-receiver WPT [6]. With the development of the WPT, the anti-misalignment in two-dimensional (2D) plates cannot satisfy the requirements of some applications in both consumer and industrial electronics, such as the three-dimensional (3D) misalignments of the WPT system on electric boats due to weather and water surface changes, as shown in Fig. 1. Thus, the 3D anti-misalignment is a valuable issue to be solved for WPT applications.

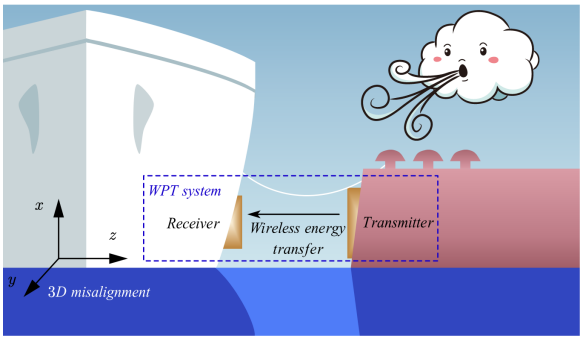

Fig. 1. 3D misalignment of WPT system on electric boat caused by weather and water surface changes.

Many research works aim to address the two-dimensional anti-misalignment at a plate by generating a uniform magnetic field through the coil design [7–17]. The sparse coils are commonly used in the research works [8–13], whose sparse structure achieves uniform field distribution by accumulating the magnetic field generated by the turns in different positions. Inner turns weaken the center field and strengthen the edge field, while outer inners have the opposite effect. The structure with anti-parallel bundles at different planes is proposed in [15]. This coil structure uses the magnetic field generated by the turns at various heights and directions to achieve uniformity. However, the anti-direction turns decrease the field strength which would decrease the transfer efficiency. In [16], the magnetic field is obtained by optimizing the width of each turn, which is printed on a printed circuit board (PCB) with copper foil. This coil structure is mainly used for applications at high frequency and low power. A coil structure composed of split parallel windings is demonstrated in [17] to generate different current amplitudes in the coil. However, the current amplitude is limited, which can only be half the original after

Manuscript created July, 2024; this work was supported in part by the Hong Kong Research Grants Council, Hong Kong Special Administrative Region, China, under Grant T23-701/20-R, in part by the Hong Kong Research Grants Council Collaborative Research Fund, Hong Kong Special Administrative Region, China, under Grant C1052-21G and in part by The Hong Kong Polytechnic University, under Grant P0048560. (*Corresponding author: Shuangxia Niu*).

Jiahua Lyu, Wei Liu, Shuangxia Niu, Tianyi Liu, Songyan Niu, and K. T. Chau are with Research Centre for Electric Vehicles and Department of Electrical and Electronic Engineering, The Hong Kong Polytechnic University, Hong Kong, China (e-mail: jiahua.lyu@connect.polyu.hk; wei.liu@polyu.edu.hk; eesxniu@polyu.edu.hk; andrew-ty.liu@connect.polyu.hk; songyan-nic.niu@polyu.edu.hk; k.t.chau@polyu.edu.hk;).

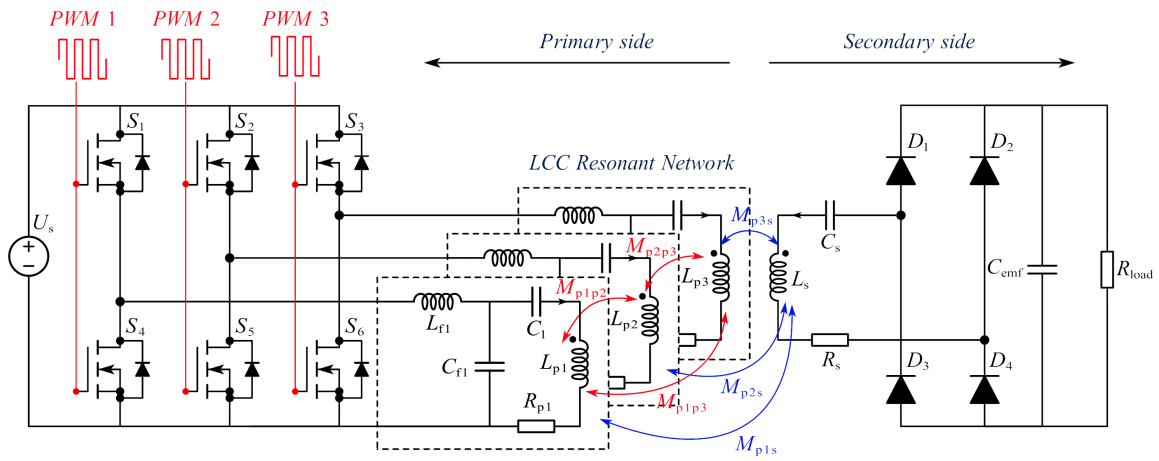

Fig. 2. Circuit diagram of the proposed multi-current modulation 3D free-positioning WPT system.

each winding split. These coil design methods have a common inconvenience in that only a constant transmission distance is allowed after one design. If the transmission distance is changed, a new design for the coil structure is required. Some hybrid compensation methods are proposed to solve the misalignment problem, and they allow some tolerance in the 3D misalignment [18, 19]. However, the WPT system proposed in [18] has weak performance in the longitude direction due to the prototype of DD coil, and the system in [19] shows poor anti-misalignment performance in three directions. Thus, it is necessary to develop a WPT system to achieve 3D anti-misalignment without changing couplers' structures.

In order to improve the 3D anti-misalignment tolerance, a multiple-current amplitude modulation scheme is proposed for the WPT system in this work. A three-layer concentric planar transmitter driven by multiple current amplitudes is developed to precisely modulate the magnetic field to achieve a uniform distribution. The proposed structure can not only achieve a better performance in the uniformity of the field distribution compared to traditional and existing designs but can also keep the uniform magnetic field at different transmission distances by adjusting the combinations of different current amplitudes. However, it would be difficult to design a suitable transmitter structure that could satisfy the uniform field distribution at various transmission distances while considering the optimal current combinations. The problem can be summarized as a bilevel optimization problem [20]: the inner-level is to find the optimal current combination at different transmission distances for each transmitter structure, and the outer-level is to optimize the transmitter structure under consideration of the inner-level. Considering the complexity of bilevel optimization and the long electromagnetic simulation calculation time, there are currently few suitable methods to optimize the structure and current amplitudes of the proposed system. A surrogate-assisted multi-fidelity genetic algorithm (SAMFGA) is proposed to address the bilevel optimization problem for transmitter structure optimization. Then the bilevel optimization problem is solved through SAMFGA, and he optimal structure and current amplitude combinations are obtained.

The primary contribution and novelty of this paper is the development of a multiple-current amplitude modulation method, which achieves 3D free-positioning WPT by modulating current amplitudes rather than redesigning the coil structure. This technique enables uniform magnetic field distribution across varying transmission distances, offering a more practical and convenient solution compared to approaches that require complex or customized coil designs. To solve the associated bilevel optimization problem, we propose a novel algorithm named SAMFGA, which efficiently determines the optimal transmitter structure and current configurations within a reasonable computational time on a personal computer. Furthermore, the proposed system is rigorously compared with traditional coil designs, including evenly distributed windings (EDW) and unevenly distributed windings (UDW), under 3D misalignment. The results highlight the limitations of existing designs, emphasizing the advantages of our approach. Finally, experimental validation demonstrates that the proposed WPT system maintains stable voltage and power levels under 3D misalignment, proving the effectiveness and practicality of the method.

The rest of the paper is arranged as follows: the circuit configuration of the proposed system is introduced in Section II. The calculation method of the magnetic flux density based on the Biot-Savart Law (BS-Law) is introduced in Section III. Then, the proposed optimization framework for the bilevel optimization problem is introduced in Section IV. The optimization result and comprehensive comparison with EDW and UDW are presented in Section V. The experimental setup and verification are implemented in Section VI. Finally, the conclusion is summarized in Section VII.

II. System Configuration

The circuit of the proposed multiple-current modulated 3D free-positioning WPT system is shown in Fig. 2. Three half-bridge converters comprised of six power transistors $S_1 - S_6$ are powered by one dc voltage source $U_\mathbf{s}$. The LCC resonant network is applied to achieve a constant coil current independent of the load and the coupling coefficient. The coil current is modulated by pulse width modulation (PWM) to reach the

optimized amplitude. In the paper, the subscript p accounts for the primary side and s accounts for the secondary side. $L_{\mathrm{f}i}$, $C_{\mathrm{f}i}$, C_i are the resonant components for each sub-circuit i, $L_{\mathrm{p}i}$ and $R_{\mathrm{p}i}$ are the self-inductance and resistance for each transmitter. M_{pp} and M_{ps} are the mutual inductance among primary sides and the mutual inductance between the primary side and the secondary side. L_{s}, R_{s} and C_{s} are the self-inductance, resistance of the receiver coil and the capacitance of the secondary compensation circuit. $D_1 - D_4$ are the diodes of the rectifier, C_{emf} is the filter capacitor, and R_{load} is the load resistance.

The simplified circuit diagram is shown in Fig. 3; the proposed system can be analyzed as a multi-input single-output (MISO) system, where U_{ac} is the output ac voltage of the half-bridge converter. The fundamental harmonic analysis (FHA) method is widely used for WPT analysis. It is due to the resonant network's ability to suppress harmonics, allowing focus on the fundamental frequency component [21]. Therefore, considering only the fundamental component, the output voltage of the i^{th} half bridge can be expressed as

$$U_{\mathrm{ac}i}(t) = \frac{2U_{\mathrm{s}}}{\pi}\sin(\omega t)\sin(\pi d_i) \tag{1}$$

where d_i is the duty circle of the the i^{th} half bridge. I_i, $I_{\mathrm{p}i}$, I_{s} in Fig. 3 are the total current, the primary coil current of each sub-circuit, and the secondary coil current. R_{eq} is the equivalent load, which can be derived from (2)

$$R_{eq} = \frac{8}{\pi^2}R_{\mathrm{load}}. \tag{2}$$

When the system works at the resonant frequency, the circuit parameters satisfies (3):

$$\omega = \frac{1}{\sqrt{L_{\mathrm{f}i}C_{\mathrm{f}i}}} = \frac{1}{\sqrt{(L_{\mathrm{p}i} - L_{\mathrm{f}i})\,C_i}} = \frac{1}{\sqrt{L_{\mathrm{s}}C_{\mathrm{s}}}}. \tag{3}$$

Based on the resonant relationship, and knowing that $L_{\mathrm{p}i}$ are the designed variables, the secondary current I_{s} can be calculated as

$$I_{\mathrm{s}} = \frac{\mathrm{j}\omega\left(\sum_{i=1}^{n} I_{\mathrm{p}i}M_{\mathrm{p}i,\mathrm{s}}\right)}{\mathrm{R_{eq}} + R_{\mathrm{s}}}. \tag{4}$$

Then, the current I_i can be solved by Kirchhoff's Law, and it can be represented by (5)

$$I_i = \mathrm{j}\omega C_{\mathrm{f}i}I_{\mathrm{p}i}Z_{\mathrm{p}}^i \tag{5}$$

where Z_{p}^i is the summation of reflected impedance from other primary coils, secondary coil, and self-resistance of coil *i*. It is shown in Fig. 3 and represented by (6)-(8)

$$Z_{\mathrm{p}}^i = Z_{\mathrm{pp}i} + Z_{\mathrm{ps}i} + R_{\mathrm{p}i} \tag{6}$$

$$Z_{\mathrm{pp}i} = \sum_{j=1,j\neq i}^{n} \frac{\mathrm{j}\omega M_{\mathrm{p}i,\mathrm{p}j}I_{\mathrm{p}j}}{I_{\mathrm{p}i}} \tag{7}$$

$$Z_{\mathrm{ps}i} = \frac{\omega^2 M_{\mathrm{p}i,\mathrm{s}}\sum_{j=1}^{n} M_{\mathrm{p}j,\mathrm{s}}I_{\mathrm{p}j}}{I_{\mathrm{p}i}\,(R_{\mathrm{eq}} + R_{\mathrm{s}})} \tag{8}$$

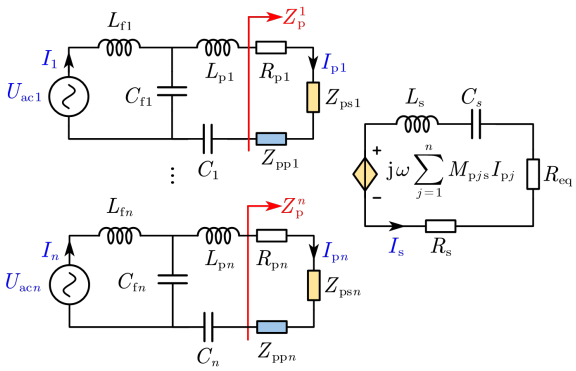

Fig. 3. Simplified circuit diagram of proposed WPT system.

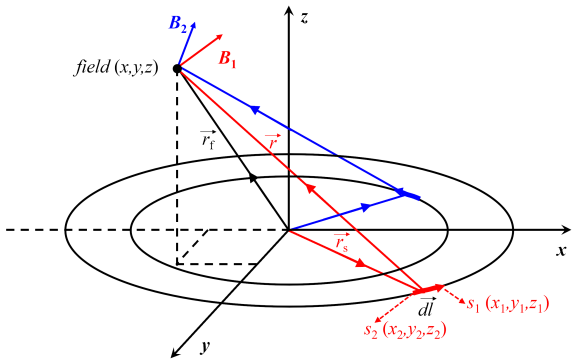

Fig. 4. Magnetic field calculation for a single point in free space by Biot-Savart Law.

where $Z_{\mathrm{pp}i}$ is the reflected impedance of the sub-primary coil *i* from other sub-primary coils, and $Z_{\mathrm{ps}i}$ is the reflected impedance from the secondary coil to the sub-primary coil *i*.

III. Magnetic Field Analysis

The finite element method (FEM) is a common tool for solving electromagnetic problems in the optimal design for WPT system [6, 22]. At the same time, the long simulation time of FEM is not convenient for the iterative optimization algorithms. For the proposed air coil which uses magnetic field uniformity as the design objective, BS-Law could determine the magnetic field rapidly and accurately.

The magnetic flux density of an arbitrary point in free space is equal to the vector sum of the magnetic fields produced by all current segments, like the field point shown in Fig. 4. The differential source segment with current is regarded as a small cylinder with length $\mathrm{d}l$, $s_1\,(x_1, y_1, z_1)$ and $s_2\,(x_2, y_2, z_2)$ are the two terminals of the source segment, like the red segment shown in Fig. 4. Thus, the differential form of BS-Law could be written as (9):

$$\mathrm{d}\boldsymbol{B} = \frac{\mu_0 I}{4\pi r^3}(\mathrm{d}\boldsymbol{l} \times \boldsymbol{r}) \tag{9}$$

where $\boldsymbol{r}$ is the vector from the source segment to the field point $field\,(x, y, z)$. Substituting the coordinates in to $\mathrm{d}\boldsymbol{l}$ and $\boldsymbol{r}$ yields:

$$\mathrm{d}\boldsymbol{l} = (x_2 - x_1)\,\boldsymbol{a_x} + (y_2 - y_1)\,\boldsymbol{a_y} + (z_2 - z_1)\,\boldsymbol{a_z} \tag{10}$$

$$\begin{aligned}\boldsymbol{r} = \boldsymbol{r_f} - \boldsymbol{r_s} = &\left(x - \frac{x_1 + x_2}{2}\right)\boldsymbol{a_x} + \left(y - \frac{y_1 + y_2}{2}\right)\boldsymbol{a_y} \\ &+ \left(z - \frac{z_1 + z_2}{2}\right)\boldsymbol{a_z}.\end{aligned} \tag{11}$$

Combining (9)-(11), the magnetic flux density in z direction $\boldsymbol{B_z}$ can be yield:

$$\begin{aligned}\mathrm{d}\boldsymbol{B_z} = \frac{\mu_0 I}{4\pi r^3}\Bigg[&(x_2 - x_1)\left(y - \frac{y_1 + y_2}{2}\right) \\ &- (y_2 - y_1)\left(x - \frac{x_1 + x_2}{2}\right)\Bigg]\boldsymbol{a_z}.\end{aligned} \tag{12}$$

$$U_{\mathrm{ind}} = \mathrm{j}\omega \iint_S \boldsymbol{B_z}\mathrm{d}S = \mathrm{j}\omega \sum M_{\mathrm{p}i,\mathrm{s}} I_{\mathrm{p}i} \tag{13}$$

The misalignment caused by coil flipping is not the point of the paper, and the receiving coil is always parallel with the transmitters. Thus, only the magnetic flux density in z direction $\boldsymbol{B_z}$ is considered. Then, the induced voltage in the secondary coil can be calculated using (13). In this work, the magnetic field analysis is further used to solve the fitness function in the optimization process instead of the mutual inductance, according to (13). The partial equivalent element method (PEEC) in [23] is adopted for the resistance and inductance calculation in the design process.

IV. Optimal Design Process

The three-layer concentric coupler structure for the multi-current modulated WPT system is proposed, as shown in Fig. 5. There are three sub-coils in the transmitter. Three sub-coils are located on three layers, and the gap between each layer is defined as g. In Fig. 5, r_{tx} and r_{rx} are the outer radius of the transmitter and receiver, z represents the transmission distance, and d represents the distance between the center points of two adjacent turns of the coil. $N_{\mathrm{t}1-3}$ represent the number of turns in each sub-coil. $N_{\mathrm{d}1}$ represents the number of turns from the second sub-coil starting position to the outer diameter of the transmitter, and $N_{\mathrm{d}2}$ represents the number of turns from the third sub-coil starting position to the outer diameter of the transmitter.

The magnetic field distribution of the three-layer coil and the contribution of each sub-coil is shown in Fig. 6, and the total field is a linear superposition of the effects of each sub-coil. The shape of the magnetic field generated by the top layer can be considered similar to traditional windings. Its characteristic is that the peak appears near the edge of the coil, and the valley appears in the middle of the coil. The function of the middle layer and the bottom layer is to reduce the peak magnetic field at the edge and fill the valley magnetic field in the middle area smoothly, as shown in Fig. 6. This is the reason why the three-layer coil structure is developed.

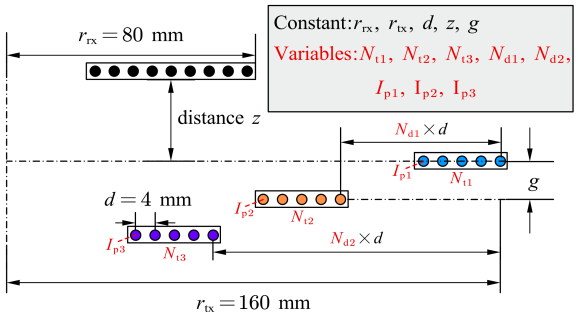

Fig. 5. Cross-section of the three-layer concentric coupler structure for proposed WPT system.

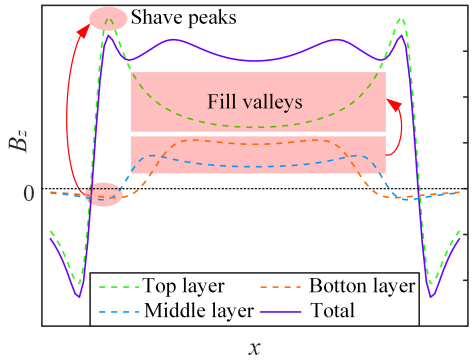

Fig. 6. Magnetic field distribution in the z-direction of the three-layer coil and the contribution of each sub-coil.

In order to achieve a consistent magnetic flux density across varying transmission distances, the design process must consider both the configuration of the coil and the precise tuning of current amplitudes. For any possible coil structure, the best current combinations need to be optimized to evaluate the anti-misalignment ability of the coil. Thus, this optimal design can be conceptualized as a bilevel optimization problem. The optimization of coil current can be regarded as an inner-level optimization problem, while the optimization of coil structure constitutes the outer-level. An optimization framework named surrogate-assisted multi-fidelity genetic algorithm (SAMFGA) is proposed to address this bilevel optimization problem. In this section, the methodology of SAMFGA and its effective implementation within the context of our proposed WPT system will be demonstrated.

A. Design Variables

The aim of the bilevel task is to find a coil structure that has good anti-misalignment performance at all transmission distances through the SAMFGA framework. Then, the optimal current amplitude combinations at various transmission distances will be found. Thus, the design variable of the bilevel optimization is the coil structure, which is defined as $\boldsymbol{x}$. $\boldsymbol{x}$ can be represented as $\boldsymbol{x} = [N_{\mathrm{t}1}, N_{\mathrm{t}2}, N_{\mathrm{t}3}, N_{\mathrm{d}1}, N_{\mathrm{d}2}]$, which includes five coil parameters and is as shown in Fig. 5. After the coil structure is determined, the variable that needs to be designed is the current modulation scheme of the coil $\boldsymbol{I} = [I_{\mathrm{p}1}, I_{\mathrm{p}2}, I_{\mathrm{p}3}]$ at different transmission distances z. It

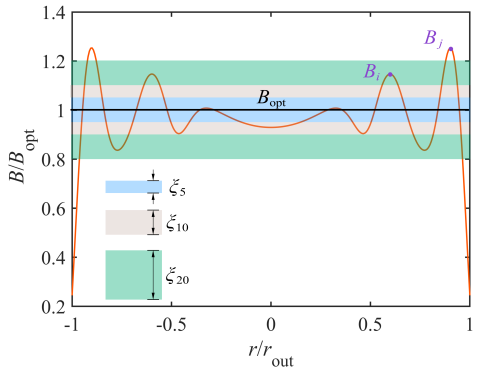

Fig. 7. Indication of fitness function with different fluctuation tolerances.

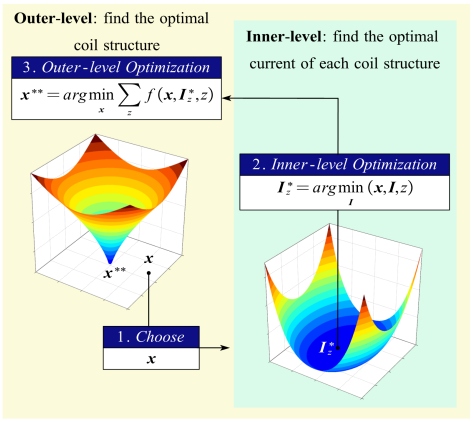

Fig. 8. Schematic diagram of the solution to the bilevel optimization problem of the proposed WPT system.

should be noted that in order to facilitate the optimization and reduce the optimization space, $\boldsymbol{I}$ is set to a decimal with a scale of 0.1.

B. Design Objective

The aim of the work is to synthesize a uniform magnetic field distribution. However, perfect uniformity is hard to achieve. Some fluctuations are allowed in the optimal design, ξ is used to represent the acceptable ripple ranges as shown in Fig. 7. ξ_n represents that the ripple is allowed to be n percent of the target value B_{opt}. The fitness function (14) is proposed to indicate the uniform performance of the coil.

$$f = \sum_{i=1} \max\left(|B_i - B_{\text{opt}}| - \xi B_{\text{opt}}, 0\right) \tag{14}$$

This indicator is initially used for filter design [24], the indicator can represent the fluctuation around the target value by one variable, instead of the commonly used mean and variance. f is an accumulation of each discrete point B_i. If the point is located within the ripple range, such as B_i for ξ_{20} in Fig. 7, its value is zero according to (14). If the point is located outside the range, like B_j in Fig. 7, it contributes to f, and the contribution depends on the deviation distance from the boundary. The optimization problem can be summarized by (15)-(16)

$$\begin{aligned} &inner\ level: \boldsymbol{I}_z^* = \arg\min_{\boldsymbol{I}} f(\boldsymbol{x}, \boldsymbol{I}, z) \\ &outer\ level: \boldsymbol{x}^{**} = \arg\min_{\boldsymbol{x}} \textstyle\sum_{z=1}^{n_{\text{case}}} f(\boldsymbol{x}, \boldsymbol{I}_z^*, z) \end{aligned} \tag{15}$$

$$\boldsymbol{I}_z^{**} = \arg\min_{\boldsymbol{I}} f(\boldsymbol{x}^{**}, \boldsymbol{I}, z). \tag{16}$$

The schematic diagram of the solution to the bilevel optimization problem of the proposed WPT system is shown in Fig. 8. It can be seen from the figure that the bilevel optimization problem has been defined as (15), and for each step in the outer level, an entire optimization needs to be conducted in the inner-level optimization. The purpose of the optimization is to find the best coil structure $\boldsymbol{x}^{**}$ through the bilevel optimization demonstrated as (15), and then obtain the optimal current combination $\boldsymbol{I}_z^{**}$ for different heights z through the original GA as shown in (16).

C. Optimization Framework

SAMFGA is developed subject to the bilevel optimization problem demonstrated in (15). The surrogate-assisted optimization (SAO) and multi-fidelity optimization (MFO) are two algorithms used for optimization solutions of complex electromagnetic problems [25]. The proposed algorithm integrates SAO, MFO, and a traditional genetic algorithm (GA) to tackle the bilevel optimization problem in the WPT system. In SAMFGA, we use an artificial neural network (ANN) to build the surrogate model. The low-fidelity GA (LFGA) involves a smaller number of populations and generations, while the high-fidelity GA (HFGA) uses a larger number of populations and generations. The inner-level optimization relies on LFGA, which allows for a quick preliminary evaluation of the comprehensive anti-misalignment capability of any structure across all transmission distances. After evaluating all coil structures using LFGA, the top-performing structures are selected for further optimization with HFGA for higher precision. After the optimal coil structure is obtained, the current modulations at various heights are solved by GA and BS-Law. The optimization framework is illustrated in Fig. 9, and the specific steps are as follows:

1) Step 1: Determine the upper and lower limits of the design variables $\boldsymbol{x}$, $\boldsymbol{I}$ and their constraints. The constraints of the optimization problem is defined in (17)

$$s.t. \begin{cases} I_{\min} \leqslant I_{\text{p1-p3}} \leqslant I_{\max} \\ N_{\text{t1}} < N_{\text{turn}} \\ N_{\text{d1}} > N_{\text{t1}} \\ N_{\text{d1}} + N_{\text{t2}} < N_{\text{turn}} \\ N_{\text{d2}} > N_{\text{d1}} + N_{\text{t2}} \\ N_{\text{d2}} + N_{\text{t3}} < N_{\text{turn}} \end{cases} \tag{17}$$

where N_{turn} is the total number of turns that can be placed on the top layer of the transmitter.

2) Step 2: Sample the input data including $\boldsymbol{x}, \boldsymbol{I}, z$ within the constraints, and evaluate their fitness values by (12) and (14). Then, build the ANN as the surrogate model by the input structure data $(\boldsymbol{x}, \boldsymbol{I}, z)$ and their evaluated fitness values $f(\boldsymbol{x}, \boldsymbol{I}, z)$.

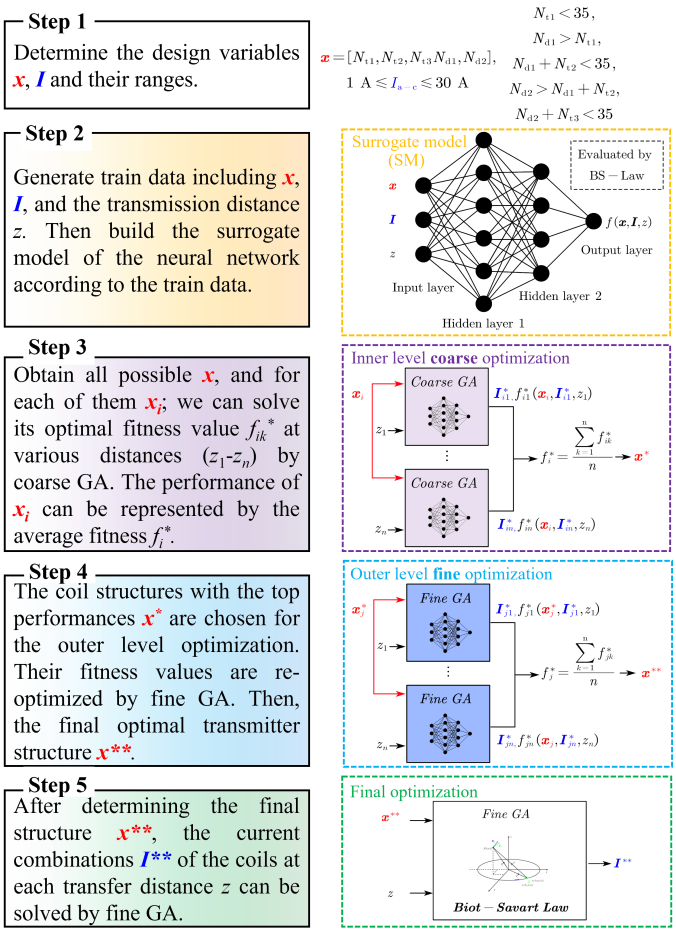

Fig. 9. Optimization flowchart for designing proposed WPT system.

3) Step 3: Obtain all possible coil structure parameters $\boldsymbol{X}$. For each of them $\boldsymbol{x}_i$, find its optimal current $\boldsymbol{I}^*_{i1-n}$ at all distances z_{1-n} through LFGA. LFGA uses GA with low populations and generations as the optimizer and using ANN as the evaluation method. LFGA ensures that each optimization takes a very short time in the inner-level loop. Then the fitness value of the structure at all distances f^*_{i1-n} can be found. The average value of the fitness values f^*_i is regarded as the preliminary performance of the structure. According to the performance f^*_i ranking, n^* of the optimal coil configurations in low-fidelity models $\boldsymbol{x}^*$ can be obtained.
4) Step 4: For each $\boldsymbol{x}^*_j$ in $\boldsymbol{x}^*$, the optimization process is the same as the previous step. It should be noted that the optimizer in HFGA uses a GA with a large population and generation. After all individuals in $\boldsymbol{x}^*$ have been optimized, the optimal coil structure $\boldsymbol{x}^{**}$ is obtained.
5) Step 5: $\boldsymbol{x}^{**}$ is considered to have excellent anti-misalignment capability in all transmission distances. For each distance z, the optimal current modulation method can be solved by a fine GA, which is evaluated by BS-Law, which ensures the accuracy of the final result. Therefore, after going through the entire optimization process, the optimal coil structure $\boldsymbol{x}^{**}$ and current modulation combination under different transmission distances $\boldsymbol{I}^{**}$ can be obtained.

TABLE I
PARAMETERS FOR PROPOSED WPT SYSTEM AND OPTIMIZATION FRAMEWORK

Parameters	Value	Parameters	Value
frequency	200 kHz	z	10-60 mm
B_{opt}	300 uT	n^*	20
$I_{\min}$	1 A	ξ	5
$I_{\max}$	20 A	Population size	40 (LFGA)
r_{tx}	160 mm		100 (HFGA)
N_{turn}	35	Generation	200 (LFGA)
d	4 mm		5000 (HFGA)

TABLE II
PARAMETERS OF OPTIMAL COIL STRUCTURE AND CURRENT AMPLITUDES WITH DIFFERENT COIL GAPS AT VARIOUS TRANSMISSION DISTANCES

Variables		g = 0 mm	g = 2.5 mm	g = 5 mm	g = 7.5 mm	g = 10 mm
$\boldsymbol{x}^{**}$		[5,5,6,5,12]	[5,6,7,5,12]	[6,11,5,8,30]	[5,5,7,6,12]	[5,5,5,8,14]
$\boldsymbol{I}^{**}$ (A)	z = 10 mm	[6,2,2]	[6.3,1.4,2.1]	[4.8,2.8,2.2]	[6.2,1.5,2.7]	[6.5,1.9,3.4]
	z = 20 mm	[8.6,1,1.9]	[8.5,1,1.8]	[6.8,2.1,2.9]	[8.4,1,2.4]	[8,1,3.2]
	z = 30 mm	[10.5,1,1.5]	[10.4,1,1.4]	[9.2,1,4]	[10.7,1,1.6]	[11,1,2.2]
	z = 40 mm	[12.5,1.1,1]	[12.4,1,1]	[11,1,1]	[12.8,1,1.1]	[13.3,1,1]
	z = 50 mm	[14.5,1,1]	[14.3,1,1]	[12.6,1,1]	[14.8,1,1]	[15.2,1,1]
	z = 60 mm	[16.3,1,1]	[15.9,1.1,1]	[14,1,1]	[16.4,1.1,1]	[16.9,1,1]

V. OPTIMIZATION RESULT AND PERFORMANCE ANALYSIS

The parameters required for the optimization are given in Table I. This section will give a discussion on the selection of coil gap g, and give a detailed comparison of the performance analysis with the traditional EDW and sparse UDW.

A. Effect of Coil Gap g

After obtaining the proposed SAMFGA algorithm, the effect of the coil gap g can be evaluated. Considering that the height of the transmission structure is limited, the maximum gap is chosen to be 10 mm. Within this range, five cases of g = 0 mm, g = 2.5 mm, g = 5 mm, g = 7.5 mm, and g = 10 mm are selected for the optimization process of SAMFGA. The optimized coil structure and current amplitudes of these five cases at various transmission distances are shown in Table II, and the fitness values of these five cases at various transmission distances are shown in Fig. 10. It can be seen from the figure that the performance of g = 0 mm (flat coil) is obviously inferior to other three-layer coil structures, as explained before. As g increases within the range, the system performance improves overall. When g reaches its maximum value of 10 mm, it performs best at all transmission distances. Since g is often limited by the coil structure and is not easy to change, g is selected as a constant of 10 mm in the following of the paper.

It can be seen from Table II that the optimal coil structure when the gap is 10 mm contains 5 turns in each sub-coil. The outer radius of the second and third sub-coil are N_{d1} and N_{d2} turns away from the maximum outer radius, respectively. The magnetic field flux density distributions under the modulation of different current combinations $\boldsymbol{I}^{**}$ at different transmission

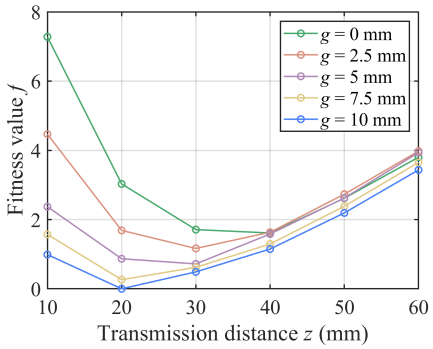

Fig. 10. Fitness values with different coil gaps g at various transmission distances.

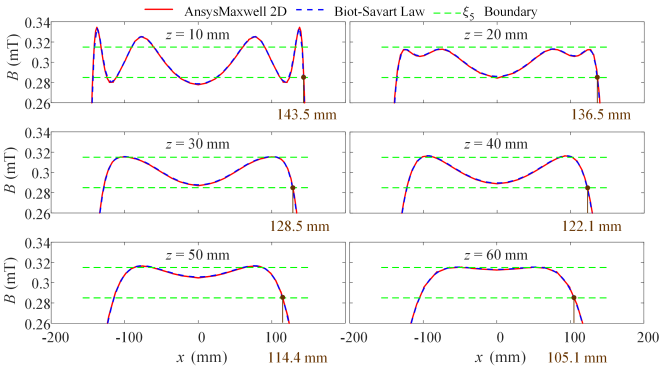

Fig. 11. Verification of calculated magnetic flux density at different transmission distances.

distances are shown in Fig. 11. To demonstrate the accuracy of the field calculated BS-Law, the simulation results by Ansys Maxwell 2D are also listed in Fig. 11 for comparison. The figure reflects that the calculated field fits well with the simulation value and that the coil designed by the BS-Law is reliable. The uniform range within the ξ_5 is marked in Fig. 11. The uniform range reduces gradually with the increase of the transmission distance.

B. Performance Analysis

To comprehensively demonstrate the 3D anti-misalignment capability, this study compares the performance of the proposed WPT system with both EDW and UDW introduced by Waffenschmidt [26]. For both winding types, comparisons are conducted using two structural approaches: variable structure (VS) and constant structure (CS). The VS approach utilizes the optimal structure for each specific transmission height, while the CS approach employs a generalized structure designed to perform efficiently across all transmission distances. A global search method is employed to determine the optimal VS and CS configurations for both EDW and UDW. For EDW, designs with current ranges from 1 A to 40 A and turn counts ranging from 1 to 30 are evaluated using the performance indicator defined in (14). For UDW, each turn is placed follows (18):

$$\frac{r\left(i\right)}{r_{\text{out}}} = \frac{1 - e^{\frac{-i}{qN}}}{1 - e^{\frac{-1}{q}}} \tag{18}$$

where $r\left(i\right)$ is the radius of the i^{th} turn, N is the total number of turns, and q is a factor related to the transmission distance. In the search process, the number of turns also varies from 1 to 30 turns. And q changes from 0 to 1 in increments of 0.01. The outer radius of the EDW and UDW is set to equal for a better comparison, and the sample range is set to 85% of the transmitter radius.

Fig. 12 illustrates the optimal field distribution at various transmission distances, while Fig. 13 lists the optimal coil parameters. The proposed coil demonstrates good anti-misalignment ability across the entire transmission range. Compared to the CS UDW, the proposed structure performs slightly better at 20-50 mm distances and significantly better at 10 mm and 60 mm. The VS UDW shows better overall

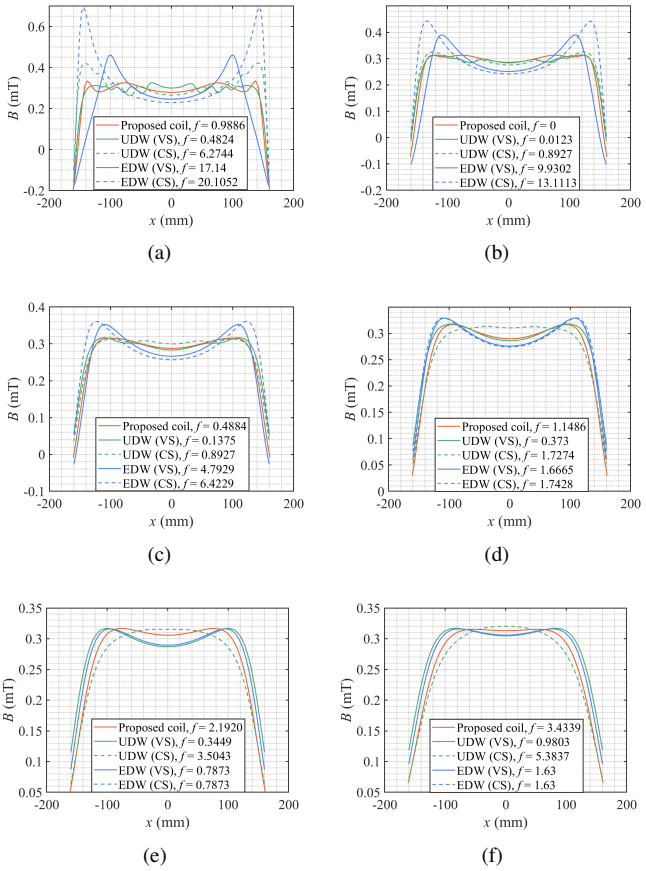

Fig. 12. Performance comparison of proposed structure with EDW and UDW from [26] at different transmission distances. (a) z = 10 mm. (b) z = 20 mm. (c) z = 30 mm. (d) z = 40 mm. (e) z = 50 mm. (f) z = 60 mm.

performance but requires structural changes (q) to achieve a uniform magnetic field at different distances. At longer distances (50-60 mm), the VS UDW needs a low q value, gathering almost all turns at the coupler edge, which is impractical. EDW with CS and VS exhibit poor magnetic field uniformity at low distances (10-30 mm) and improved performance at higher distances (40-60 mm). However, Fig. 13 shows that higher distances require fewer turns N, leading to lower mutual inductance and transmission efficiency. This comparative

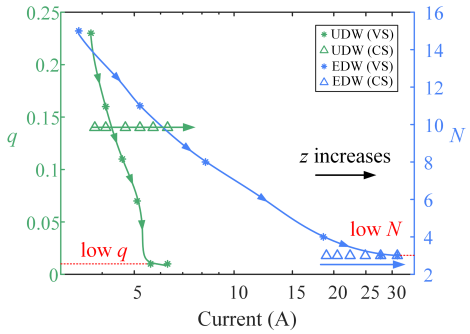

Fig. 13. Optimal coil parameters of EDW and UDW from at different transmission distances.

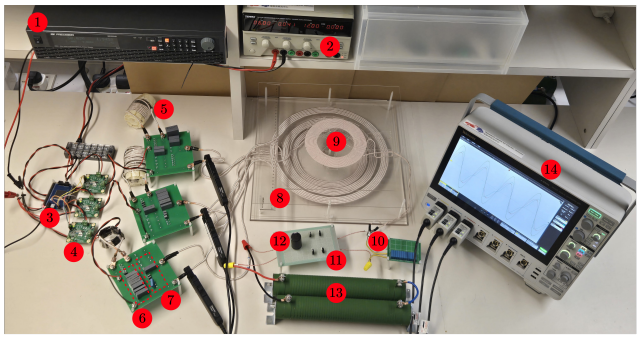

1. DC power source 2. DC driving source 3. DSP 4. GaN half-bridge converter 5. L_f 6. C_f 7. C 8. Transmitter ($L_{p1\text{-}3}$) 9. Receiver (L_s) 10. C_s 11. Rectifier 12. C_{emf} 13. Load 14. Oscilloscope

Fig. 14. Configuration of the experimental setup.

analysis demonstrates that the proposed system achieves comprehensive 3D anti-misalignment capability across different transmission distances without structural changes, which is a significant improvement compared with previous methods.

VI. Experimental Verification and Benchmark

The proposed WPT system's performance is verified through experimental implementation. The setup illustrated in Fig. 14 utilizes an LCC compensation network that maintains constant transmitter current independent of load and coupling coefficient. Three half-bridge inverters powered simultaneously by a dc source modulate the current flow through three sub-coils. All relevant circuit parameters are detailed in Table III.

TABLE III
Values of System Parameters for the Experimental Verification

Symbol	Value	Symbol	Value	Symbol	Value	Symbol	Value
L_{f1}	1.77 uH	L_{p1}	16.846 uH	R_{f1}	0.094 Ω	M_{p1p2}	6.47 uH
L_{f2}	11.3 uH	L_{p2}	12.7 uH	R_{f2}	0.05 Ω	M_{p1p2}	3.52 uH
L_{f3}	8.2 uH	L_{p3}	9.255 uH	R_{f3}	0.034 Ω	M_{p2p3}	5.35 uH
C_{f1}	375.4 nF	C_1	41.9 nF	R_{p1}	0.14 Ω	L_s	41.7 uH
C_{f2}	56.1 nF	C_2	477.1 nF	R_{p2}	0.06 Ω	C_s	15.2 nF
C_{f3}	77.8 nF	C_3	611.3 nF	R_{p3}	0.04 Ω	R_s	0.12 Ω
S_{1-6}	EPC2001C	D_{1-4}	STPS20120D	C_{emf}	2200 nF	R_{load}	20 Ω

The system is designed to maintain a constant 30 V output regardless of horizontal misalignment or transmission distance. In order to achieve 3D anti-misalignment capability, the transmitter currents are modulated proportionally according to Table II at varying distances. Fig. 15 displays the current waveforms of the sub-coils at six selected transmission distances (10 mm to 60 mm) with RMS values indicated. The observed current ratios in different combinations closely align with those specified in Table II, confirming the system's effectiveness. It can be seen from Fig. 15 that the current in the primary coil is distorted. This may be due to the interference of the harmonics in the three sub-channels. This phenomenon can be alleviated if three independent power supplies are used to drive each sub-channel separately.

Fig. 16 illustrates the output voltage under horizontal misalignment at various transmission distances. For distances between 10 to 40 mm, the system demonstrates excellent horizontal anti-misalignment ability with minimal output voltage

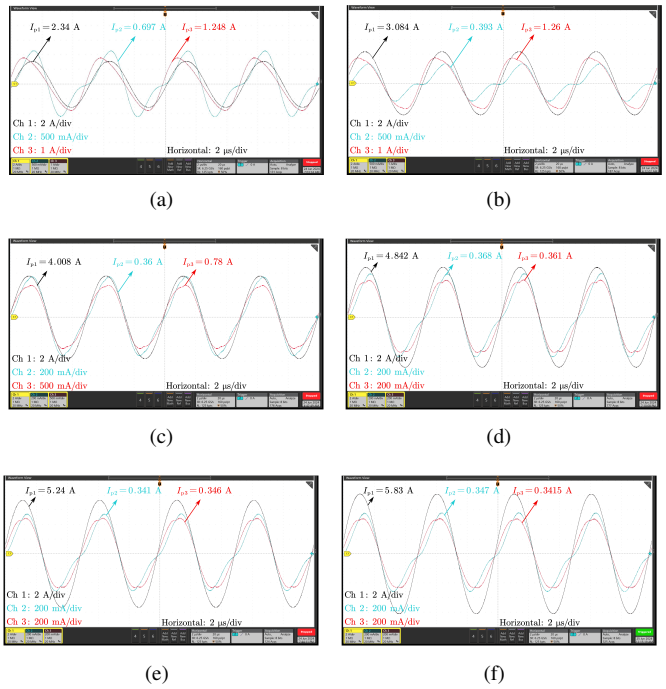

Fig. 15. Current waveforms of each coil ($I_{p1} - I_{p3}$) at different transmission distances z. (a) z = 1 cm. (b) z = 2 cm. (c) z = 3 cm. (d) z = 4 cm. (e) z = 5 cm. (f) z = 6 cm.

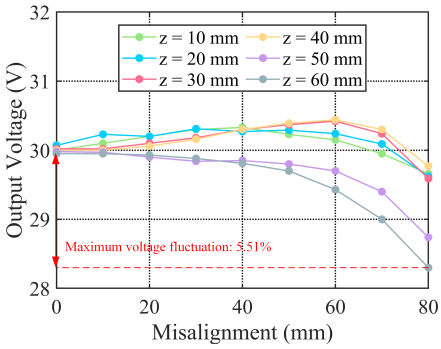

Fig. 16. Experimental measurement of the output voltage under 3D misalignment.

fluctuations around the target voltage. At distances of 50 to

TABLE IV
ANTI-MISALIGNMENT CAPABILITY BENCHMARK OF EXISTING RESEARCH WORK

Ref	Dimension (mm) TX	Dimension (mm) RX	Air Gap (mm)	Maximum Efficiency (%)	Misalignment Tolerance(%) x	Misalignment Tolerance(%) y	Misalignment Tolerance(%) z	Output Fluctuation(%) Voltage	Output Fluctuation(%) Power	Output Power (W)
[27]	200*200	200*200	100	86	11	30	-	5	-	105
[18]	775*391	775*391	100-140	93	15.5	40.9	10.2	-	5	3300
[19]	60	44	2-8	79	8.3	8.3	10	9	-	35
[28]	350	350	175	94.46	28.6	28.6	-	9	-	3300
[29]	400	200	100	90.27	25	25	-	-	3	227
[30]	400	65	80	92.2	33.8	33.8	-	5	-	700
[31]	153	95	6-20	86.48	32.7	32.7	10.5	31	-	100
[32]	1100*900	700*300	100-200	75	36.4	18.2	9.1	29	-	15600
This Work	320	160	10-60	83.2	**25**	**25**	**15.6**	5.51	11.8	45

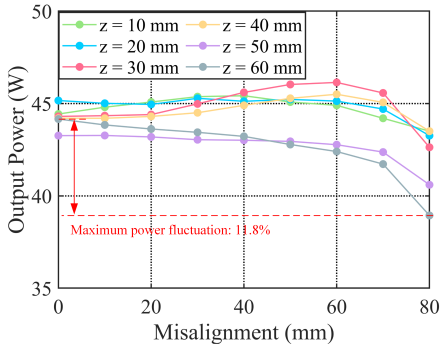

Fig. 17. Experimental measurement of the output power under 3D misalignment.

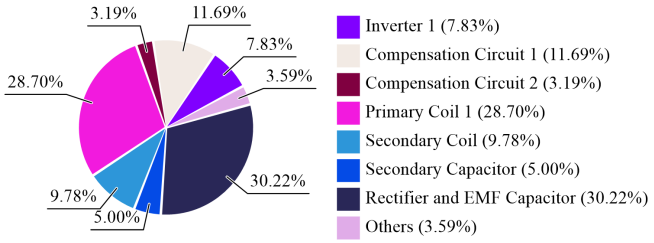

Fig. 18. Loss breakdown of the proposed WPT system at z = 40 mm.

60 mm, output fluctuations increase with misalignment. The largest fluctuation of 5.51% occurs at a 60 mm transmission distance. Fig. 17 shows similar trends in output power changes. The maximum power fluctuation of 11.8% is observed at 80 mm horizontal misalignment with a 60 mm transmission distance. Both voltage and power fluctuations remain within acceptable ranges. These results demonstrate that the proposed wireless charging system achieves varying degrees of anti-misalignment capability by modulating coil current without structural changes. When the receiver aligns to the center of the transmitter with the transmission distances varying from 10 to 60 mm, the system efficiencies are 83.2%, 82.2%, 82.7%, 81.8%, 79.5%, and 77.8%, respectively. The power transfer efficiency is acceptable for the proposed WPT system without ferrite [6, 33–35].

Since the efficiency does not change much when the transmission distance changes, the loss breakdown is evaluated by the oscilloscope and probes when the transmission distance is 40 mm, as shown in Fig. 18. It can be seen from the figure that the largest loss is in the rectification and filtering part, followed by the primary coil 1 and its compensation circuit. Since the loss of the rectification part is relatively fixed, in future work, the power of the system can be increased to reduce the proportion of the loss of the rectifier part and thus improve the efficiency of the system. At the same time, more efficient litz wires can be used to reduce the loss of the primary coil 1 and its compensation circuit to increase the efficiency of the system.

Table IV benchmarks existing research on anti-misalignment capabilities in WPT systems. Circular coils demonstrate horizontal anti-misalignment ability with equal performance on x- and y-axes. The proposed coil structure improves z-axis misalignment tolerance to 15.6% while maintaining a 25% misalignment tolerance on the x- and y-axes, exhibiting excellent comprehensive anti-misalignment capabilities while maintaining low voltage fluctuations. Existing works [27–30] have good planar anti-misalignment capability and low output fluctuation but lack vertical anti-misalignment capability compared to the proposed work; [18, 19] have three-dimensional anti-misalignment capability and slight output fluctuation but have limitations in anti-misalignment; [31, 32] have excellent three-dimensional anti-misalignment capability but their output fluctuations are large. These results highlight the advantages of the modified structure over existing methods in achieving 3D anti-misalignment.

VII. CONCLUSION

This work presents a WPT system using multiple-current amplitude modulation to achieve 3D anti-misalignment without altering the transmitter structure. A surrogate-based optimization framework determines optimal current combinations for various transmission distances. The design method's accuracy is verified through simulation software, and the proposed structure's performance is comprehensively compared to that of EDW and UDW. Experimental validation demonstrates the system's 3D anti-misalignment capabilities with subsequent result analysis. The results reflect that the proposed WPT system allows tolerances of 25%, 25%, and 15.6% in the

x, y, and z directions, respectively, within a maximum voltage fluctuation of 5.51%. A benchmark of existing research highlights the proposed coil's balanced performance across three dimensions. This multi-current modulated WPT scheme offers a novel approach to enhancing 3D anti-misalignment in WPT systems. In future work, the decoupling methodology of multiple transmission coils can be explored, and real-time control functionality can be incorporated.

REFERENCES

[1] Y. Jang and M. M. Jovanovic, "A contactless electrical energy transmission system for portable-telephone battery chargers," *IEEE Transactions on Industrial Electronics*, vol. 50, no. 3, pp. 520–527, Jun. 2003.

[2] T. Sasatani, A. P. Sample, and Y. Kawahara, "Room-scale magnetoquasistatic wireless power transfer using a cavity-based multimode resonator," *Nature Electronics*, vol. 4, no. 9, pp. 689–697, Sep. 2021.

[3] W. Han, K. T. Chau, C. Jiang, W. Liu, and W. H. Lam, "Design and analysis of quasi-omnidirectional dynamic wireless power transfer for fly-and-charge," *IEEE Transactions on Magnetics*, vol. 55, no. 7, pp. 1–9, Jul. 2019.

[4] J. Guo, K. T. Chau, W. Liu, Y. Hou, and W. Chan, "Pulse magnitude modulation and token rotation-based voltage balancing method of multilevel inverter for wireless power transfer," *IEEE Transactions on Power Electronics*, 2024.

[5] C. Qiu, K. T. Chau, T. W. Ching, and C. Liu, "Overview of wireless charging technologies for electric vehicles," *Journal of Asian Electric Vehicles*, vol. 12, no. 1, pp. 1679–1685, Jun. 2014.

[6] S. B. Lee, M. Kim, and I. G. Jang, "Determination of the optimal resonant condition for multireceiver wireless power transfer systems considering the transfer efficiency and different rated powers with altered coupling effects," *IEEE Journal of Emerging and Selected Topics in Power Electronics*, vol. 9, no. 2, pp. 2384–2393, Mar. 2020.

[7] Y. Chen, S. Niu, W. Fu, and H. Lin, "Modelling of negative equivalent magnetic reluctance structure and its application in weak-coupling wireless power transmission," *Nature Communications*, vol. 15, no. 1, p. 6135, Jul. 2024.

[8] J. J. Casanova, Z. N. Low, J. Lin, and R. Tseng, "Transmitting coil achieving uniform magnetic field distribution for planar wireless power transfer system," in *2009 IEEE Radio and Wireless Symposium*, pp. 530–533. IEEE, May. 2009.

[9] R. He, P. Zhao, G. Ning, K. Yue, Y. Liu, and M. Fu, "Optimal driving and loading scheme for multiple-receiver inductive power transfer," *IEEE Transactions on Industrial Electronics*, vol. 69, no. 12, pp. 12 665–12 675, Dec. 2021.

[10] C. Rong, X. He, Y. Wu, Y. Qi, R. Wang, Y. Sun, and M. Liu, "Optimization design of resonance coils with high misalignment tolerance for drone wireless charging based on genetic algorithm," *IEEE Transactions on Industry Applications*, vol. 58, no. 1, pp. 1242–1253, Feb. 2021.

[11] X. Liu and S. Hui, "Optimal design of a hybrid winding structure for planar contactless battery charging platform," *IEEE Transactions on Power Electronics*, vol. 23, no. 1, pp. 455–463, Jan. 2008.

[12] Y. Zhang, N. Zhang, G. Pan, B. Yang, S. Zhou, and S. Wang, "Optimal design of coupling coils for wireless power transfer system featuring high misalignment tolerance," in *The proceedings of the 16th Annual Conference of China Electrotechnical Society*, pp. 1–10. Springer, Apr. 2022.

[13] X. Huang, W. Chen, and Q. Chen, "A design algorithm of circular transmitting coil to achieve uniform magnetic field distribution in WPT applications," in *2015 IEEE 2nd International Future Energy Electronics Conference (IFEEC)*, pp. 1–5, Dec. 2015.

[14] W. Zhou, B. Han, J. Wang, D. Wu, F. Zhao, and N. Li, "Design of uniform magnetic field coil by quasi-elliptic function fitting method with multiple optimizations in miniature atomic sensors," *IEEE Transactions on Industrial Electronics*, vol. 69, no. 11, pp. 11 755–11 764, Nov. 2021.

[15] W. Wang, C. Xu, C. Zhang, and J. Yang, "Optimization of transmitting coils based on uniform magnetic field for unmanned aerial vehicle wireless charging system," *IEEE Transactions on Magnetics*, vol. 57, no. 6, pp. 1–5, Jun. 2021.

[16] Q. Xu, Q. Hu, H. Wang, Z. H. Mao, and M. Sun, "Optimal design of planar spiral coil for uniform magnetic field to wirelessly power position-free targets," *IEEE Transactions on Magnetics*, vol. 57, no. 2, pp. 1–9, Dec. 2020.

[17] J. Li, R. Qin, J. Sun, and D. Costinett, "Systematic design of a 100-W 6.78-MHz wireless charging station covering multiple devices and a large charging area," *IEEE Transactions on Power Electronics*, vol. 37, no. 4, pp. 4877–4889, Apr. 2021.

[18] L. Zhao, D. J. Thrimawithana, U. K. Madawala, A. P. Hu, and C. C. Mi, "A misalignment-tolerant series-hybrid wireless EV charging system with integrated magnetics," *IEEE Transactions on Power Electronics*, vol. 34, no. 2, pp. 1276–1285, Feb. 2019.

[19] D. Bui, Q. Zhu, L. Zhao, and A. P. Hu, "Concentric-coil hybrid IPT system with improved tolerance to coupling and load variations," *IEEE Journal of Emerging and Selected Topics in Power Electronics*, vol. 10, no. 4, pp. 4913–4922, Aug. 2022.

[20] A. Sinha, P. Malo, and K. Deb, "A review on bilevel optimization: From classical to evolutionary approaches and applications," *IEEE Transactions on Evolutionary Computation*, vol. 22, no. 2, pp. 276–295, Apr. 2018.

[21] Y. Chen, H. Zhang, C. S. Shin, C. H. Jo, S. J. Park, and D. H. Kim, "An efficiency optimization-based asymmetric tuning method of double-sided LCC compensated WPT system for electric vehicles," *IEEE Transactions on Power Electronics*, vol. 35, no. 11, pp. 11 475–11 487, Nov. 2020.

[22] R. Bosshard and J. W. Kolar, "Multi-objective optimization of 50 kW/85 kHz IPT system for public transport," *IEEE Journal of Emerging and Selected Topics in Power Electronics*, vol. 4, no. 4, pp. 1370–1382, Dec. 2016.

[23] J. Lyu, H. C. Chen, Y. Du, and Q. S. Cheng, "Litzimp: A fast impedance extraction algorithm for litz wire coil," *IEEE Transactions on Industrial Electronics*, vol. 70, no. 9, pp. 9326–9335, Sep. 2022.

[24] Y. Yu, B. Liu, Y. Wang, and Q. S. Cheng, "Automated diplexer design with key performance indicator-based objectives," *IEEE Microwave and Wireless Components Letters*, vol. 32, no. 7, pp. 827–830, Jul. 2022.

[25] J. Lyu, H. C. Chen, Q. S. Cheng, Y. Zhang, and Y. Du, "Rapid design of litz wire using surrogate assisted optimization embedding adjacent trust region," *IEEE Transactions on Components, Packaging and Manufacturing Technology*, vol. 14, no. 12, pp. 2211–2219, Dec. 2024.

[26] E. Waffenschmidt, "Homogeneous magnetic coupling for free positioning in an inductive wireless power system," *IEEE Journal of Emerging and Selected Topics in Power Electronics*, vol. 3, no. 1, pp. 226–233, Mar. 2014.

[27] P. Yadav and M. Veerachary, "Modified coupler with reduced misalignment issues for wireless power transfer system," *IEEE Transactions on Industry Applications*, 2024.

[28] Y. Yao, A. U. Ibrahim, and W. Zhong, "A three-resonator wireless power transfer system with constant-output feature within a misalignment range," *IEEE Transactions on Power Electronics*, vol. 37, no. 12, pp. 15 753–15 763, Dec. 2022.

[29] Z. Dong, X. Li, S. Liu, Z. Xu, and L. Yang, "A novel all-direction antimisalignment wireless power transfer system designed by truncated region eigenfunction expansion method," *IEEE Transactions on Power Electronics*, vol. 36, no. 11, pp. 12 456–12 467, Nov. 2021.

[30] Z. Li, X. Li, Y. Zhou, Y. Liu, and M. Ban, "Improving misalignment tolerance for the wireless charging system using multiple coils coupler," *IEEE Transactions on Power Electronics*, vol. 39, no. 6, pp. 7721–7735, 2024.

[31] C. Zheng, H. Ma, J.-S. Lai, and L. Zhang, "Design considerations to reduce gap variation and misalignment effects for the inductive power transfer system," *IEEE Transactions on Power Electronics*, vol. 30, no. 11, pp. 6108–6119, Nov. 2015.

[32] S. Y. Choi, J. Huh, W. Y. Lee, and C. T. Rim, "Asymmetric coil sets for wireless stationary ev chargers with large lateral tolerance by dominant field analysis," *IEEE Transactions on Power Electronics*, vol. 29, no. 12, pp. 6406–6420, Dec. 2014.

[33] J. J. Casanova, Z. N. Low, and J. Lin, "A loosely coupled planar wireless power system for multiple receivers," *IEEE Transactions on Industrial Electronics*, vol. 56, no. 8, pp. 3060–3068, Jun. 2009.

[34] G. Rituraj, B. K. Kushwaha, and P. Kumar, "A unipolar coil arrangement method for improving the coupling coefficient without ferrite material in wireless power transfer systems," *IEEE Transactions on Transportation Electrification*, vol. 6, no. 2, pp. 497–509, May. 2020.

[35] S. Niu, R. Lyu, J. Lyu, K. T. Chau, W. Liu, and L. Jian, "Optimal resonant condition for maximum output power in tightly-coupled wpt systems considering harmonics," *IEEE Transactions on Power Electronics*, 2024.